NRC Research Press

ARTICLE

Warmer–wetter climate drives shift in δD–$\delta^{18}O$ composition of precipitation across the Queen Elizabeth Islands, Arctic Canada

Luke Copland, Denis Lacelle, David Fisher, Frances Delaney, Laura Thomson, Brittany Main, and David Burgess

Abstract: We examine how recent increases in air temperature and precipitation, together with reductions in sea ice extent, may have affected the regional δD–$\delta^{18}O$ composition of precipitation. In spring 2014, 80 snow samples were collected from six glaciers and ice caps across the Queen Elizabeth Islands, and in 2009 and 2014, two shallow ice cores were collected from Agassiz Ice Cap and White Glacier, respectively. The snow samples showed average $\delta^{18}O$ values from 2013 to 2014 to be approximately 2‰–3‰ higher than those recorded in 1973–1974 in nearby locations, with the ice cores showing similar trends in $\delta^{18}O$ values. A zonal average water isotope model was used to help understand the causes of the increased $\delta^{18}O$ values, using inputs calibrated for observed changes in temperature, vapour flux, and sea ice extent. Model results indicate that atmospheric temperature changes account for <1‰ of the observed change in $\delta^{18}O$ values, and that changes in local water input and precipitation driven by changes in sea ice extent only have an effect in coastal regions. Enhanced meridional vapour flux to the Queen Elizabeth Islands is, therefore, also required to explain the observed increases in $\delta^{18}O$ values, with fluxes ~7% higher today than in the 1970s, consistent with the change in precipitation.

Key words: oxygen isotopes, snow, ice cores, climate change.

Résumé : Les auteurs examinent comment les récentes augmentations de la température de l'air et des précipitations combinées aux réductions de l'étendue de la glace de mer ont pu affecter la composition régionale en δD–$\delta^{18}O$ des précipitations. Au printemps 2014, 80 échantillons de neige ont été prélevés sur six glaciers et calottes glaciaires à travers les îles de la Reine-Élisabeth, et en 2009 et 2014, deux carottes de glace peu profondes ont été prélevées respectivement sur la calotte glaciaire Agassiz et le glacier White. Les échantillons de neige ont montré que les valeurs moyennes de $\delta^{18}O$ pour 2013–14 étaient environ 2–3 ‰ plus élevées que celles enregistrées en 1973–74 dans des endroits à proximité, les carottes de glace montrant des tendances similaires quant aux valeurs de $\delta^{18}O$. Un modèle de moyenne zonale des isotopes de l'eau a été utilisé pour aider à comprendre les causes de l'augmentation des valeurs de $\delta^{18}O$, en utilisant des entrées calibrées pour les changements observés dans la température, le flux de vapeur et l'étendue de la glace de mer. Les résultats du modèle indiquent que les changements de température atmosphérique représentent <1 ‰ de la variation observée des valeurs de $\delta^{18}O$, et que les

Received 10 April 2020. Accepted 21 July 2020.

L. Copland, D. Lacelle, F. Delaney, and B. Main. Department of Geography, Environment and Geomatics, University of Ottawa, Ottawa, ON K1N 6N5, Canada.
D. Fisher. Department of Earth Sciences, University of Ottawa, Ottawa, ON K1N 6N5, Canada.
L. Thomson. Department of Geography and Planning, Queen's University, Kingston, ON K7L 3N6, Canada.
D. Burgess. Natural Resources Canada, Ottawa, ON K1A 0E8, Canada.
Corresponding author: Luke Copland (e-mail: luke.copland@uottawa.ca).

changements de l'apport local en eau et des précipitations dus aux changements de l'étendue de la glace de mer n'ont un effet que dans les régions côtières. Un flux de vapeur méridional accru vers les îles de la Reine-Élisabeth est donc également nécessaire pour expliquer les augmentations observées des valeurs de $\delta^{18}O$, avec des flux ~7 % plus élevés aujourd'hui que dans les années 1970, ce qui correspond au changement des précipitations. [Traduit par la Rédaction]

Mots-clés : isotopes d'oxygène, neige, carottes de glace, changement climatique.

Introduction

Over the past several decades, the Queen Elizabeth Islands (QEI) of the Canadian High Arctic have experienced warmer and wetter climate conditions (Mekis and Hogg 1999), such as an increase in mean annual air temperature of 3.6 °C on northern Ellesmere Island between 1948 and 2016 (White and Copland 2018), and an increase in precipitation of ~10% at Eureka between 1961 and 2007 (Lesins et al. 2010). In response to the warmer–wetter climate, there have been marked changes to various components of the cryosphere (Derksen et al. 2012). For example, sea level contributions from Canadian Arctic glaciers were approximately four times greater over the period 2005–2015 than 1986–2005 (Box et al. 2018), primarily due to increased surface runoff (Sharp et al. 2011; Harig and Simons 2016; Millan et al. 2017). Ice core records also show that recent melt rates on QEI ice caps are at their greatest in the past 9000 years (Fisher et al. 2012). Sea ice extent, age, and thickness have also experienced marked declines, with average Arctic Ocean sea ice thickness declining by ~66% over the past 60 years and multi-year sea ice reducing in area by >50% over the period 1999–2017 (Kwok 2018).

Despite many studies documenting the response of various components of the cryosphere in the QEI to changing climate, few have examined how the warmer–wetter climate and the reduction in sea ice extent may have affected the regional δD–$\delta^{18}O$ composition of precipitation, a commonly used proxy of air temperature (Dansgaard 1964; Lorius and Merlivat 1977). Between 1971 and 1974, Koerner (1979) and Koerner and Russell (1979) conducted extensive snow surveys on Axel Heiberg, Devon, and Ellesmere islands and found that distance from moisture source (i.e., Rayleigh distillation following rainout) was most influential in determining $\delta^{18}O$ values of precipitation in the QEI, although there were also significant local complexities due to site elevation, humidity, and wind scouring of snow. To improve understanding of the controls on stable isotopes in precipitation at regional and global scales, Fisher (1990, 1992) developed a global zonally averaged water isotope model that used as input zonal averages of air and sea temperatures, wind speed, relative humidity, sea ice extent, evaporation, meridional water vapour flux, and supersaturation in clouds as a function of temperature. This model was used to simulate $\delta^{18}O$ and d (deuterium excess) values in precipitation in the QEI using 1950–1980 climate normal conditions and found a good fit with 1973–1974 $\delta^{18}O$ snow transect values reported by Koerner (1979).

The objectives of this study are to (1) determine the contemporary $\delta^{18}O$ and d composition of precipitation in the QEI, and (2) identify how the relative importance of the factors affecting the $\delta^{18}O$ and d composition of precipitation across the QEI have changed over the past several decades. Regional $\delta^{18}O$ patterns are determined from 80 snow samples collected from glaciers and ice caps across the QEI in spring 2014, and compared with the 1971–1974 measurements reported by Koerner (1979) and Koerner and Russell (1979). Temporal changes in $\delta^{18}O$ and d in precipitation are assessed from differences in $\delta^{18}O$ and d values in shallow ice cores dating to the 1940s recovered from Agassiz Ice Cap and White Glacier, situated on the eastern and western side of the QEI, respectively. Finally, the inputs of the Fisher (1990) model are updated with 1980–2010 climate normal conditions

Fig. 1. Map of snow and ice core sample locations in the Queen Elizabeth Islands: (A) Meighen Ice Cap, (B) White Glacier (core WG14), (C) South Melville Ice Cap, (D) Grise Fiord Glacier, (E) Devon Ice Cap, (F) Agassiz Ice Cap (core A09). Blue dots indicate average $\delta^{18}O$ values of the 2013–2014 snowpack at sample locations in this study (± indicates standard deviation), red triangles and contour lines indicate 1973–1974 snow sample values measured by Koerner (1979). Dotted line shows the vapour trajectory used for the zonal water average isotope model shown in Fig. 6, divided into northwestern (NW) and southeastern (SE) segments. Base map created in ESRI ArcGIS 10.7 from the IBCAO v3 (Jakobsson et al. 2012).

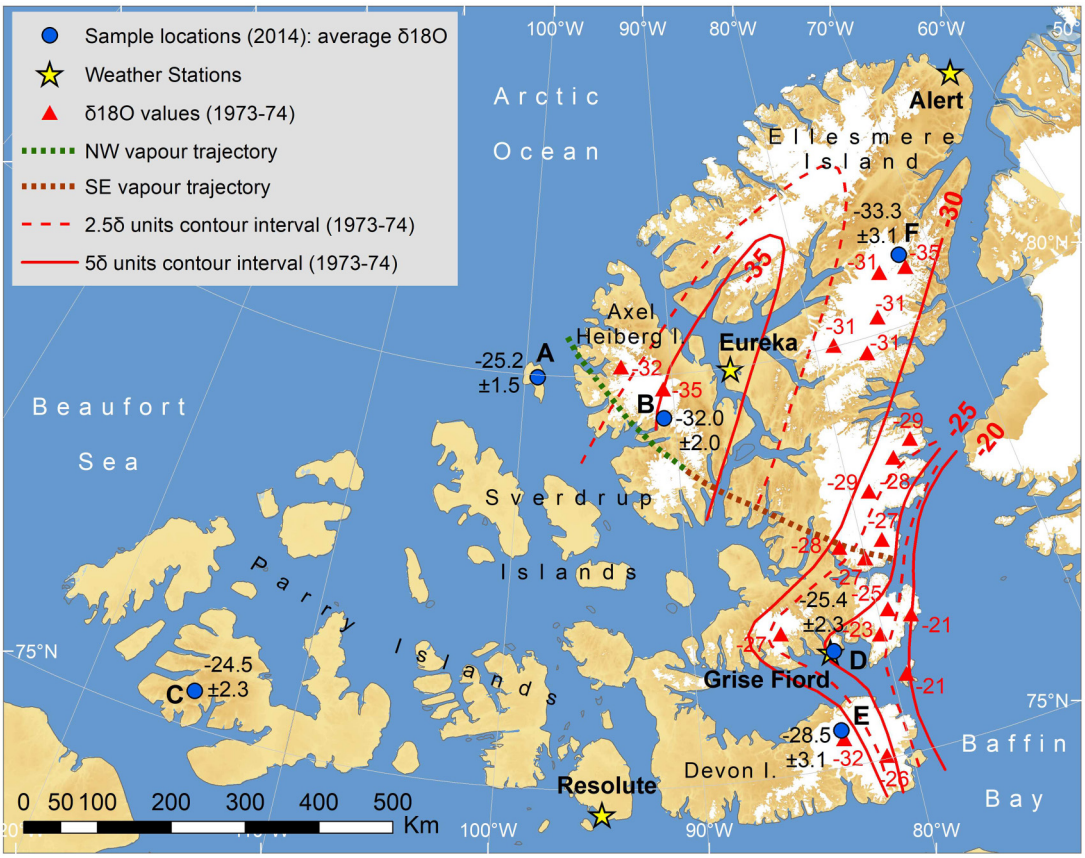

to evaluate the effects of changing sea ice extent and meridional vapour flux on changes in $\delta^{18}O$ and *d* of precipitation in the QEI.

Study area

The QEI occupies ~400 000 km^2 of land, of which ~100 000 km^2 is covered by glaciers and ice caps (Fig. 1) (Sharp et al. 2014; Marsh 2015). The major surrounding water bodies are the Arctic Ocean to the north, Beaufort Sea to the west, and Baffin Bay to the east. The QEI are mountainous over many of the ocean-facing portions of Ellesmere, Devon, and Axel Heiberg Islands, but they are generally flat and low lying over locations such as Melville, Prince Patrick, and Ellef Ringnes Islands to the west. Glaciers and ice caps are concentrated in mountainous regions along eastern and northern Ellesmere Island (elevations up to 2616 m above sea level (a.s.l.)), and western Axel Heiberg Island (elevations up to 2210 m a.s.l.). Their distribution reflects the topography and dominance of marine moisture sources in this region.

Fig. 2. Annual (A) mean air temperature, and (B) total precipitation, over the period 1948–2015 at the five climate stations with the longest available records within and adjacent to the Queen Elizabeth Islands. Source: Environment Canada (2015).

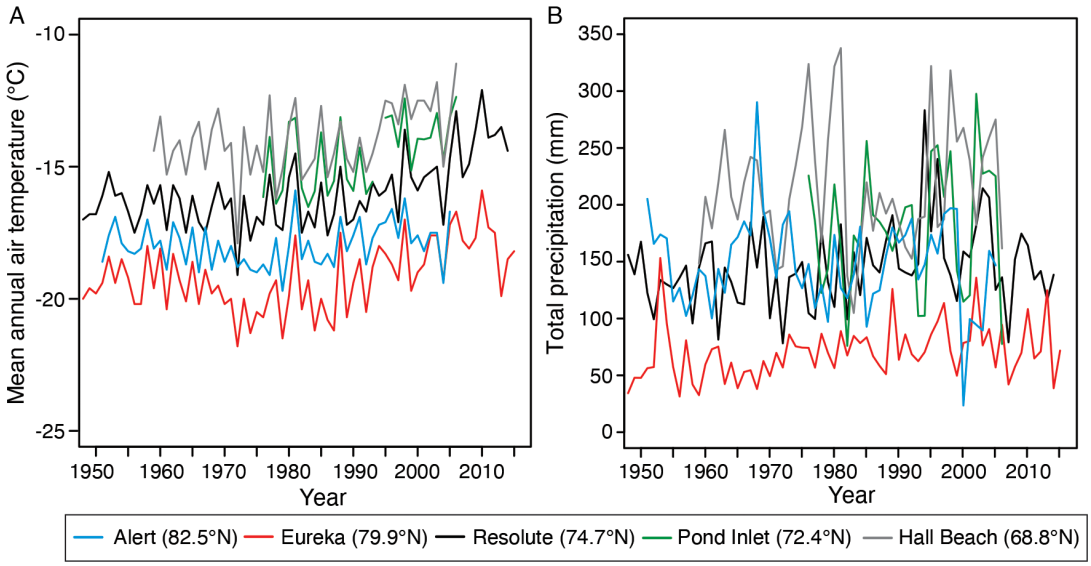

The climate of the QEI is highly variable due to its large spatial extent, varied topography, and the effects of proximity to oceans. Coastal regions all experience summer air temperatures above 0 °C, whereas high elevation regions, including near the summit of ice caps, rarely experience above-freezing temperatures. The 1950–2010 mean annual air temperature (MAAT) at Alert (82.5°N; 65 m a.s.l.), Eureka (79.9°N; 10 m a.s.l.), Resolute Bay (74.7°N; 68 m a.s.l.), Pond Inlet (72.4°N; 62 m a.s.l.), and Hall Beach (68.8°N; 9 m a.s.l.) ranged between −19.3 °C and −13.9 °C (Environment Canada 2015; Fig. 2). All stations showed strong inter-annual variations and experienced a general decrease in MAAT from the 1950s to the mid-1970s. This cooling was followed by a statistically significant increase in MAAT at a rate of 0.37 to 0.88 °C decade^{-1} over the period 1970–2010, with most warming occurring in the fall and winter.

The QEI receives low annual precipitation (~100–300 mm a^{-1}), with 60%–90% falling as snow, particularly over the interior regions in the far north; however, the east-facing slopes surrounding Baffin Bay receive higher amounts (300–1000 mm a^{-1}) (Koerner 1979). The precipitation gradient occurs due to air masses moving mainly from the Baffin Bay area north–northwest across the QEI. Across the region, precipitation increased at a rate of 2.6% decade^{-1} to 5.5% decade^{-1} over the period 1950–2010 (Environment Canada 2015) (Fig. 2).

Methods

Water isotope composition of precipitation in the QEI

In the QEI, the $\delta^{18}O$ and δD ($\delta^{2}H$) composition of local precipitation is temporally variable, and the slope values of local precipitation deviate from that of the global meteoric water line (GMWL), which was defined by Craig (1961) as

$$\delta D = 8\delta^{18}O + 10 \quad (1)$$

The GMWL represents the average of many local meteoric water lines (LMWL) that have different slope and intercept due to varying climates. The Global Network for Isotopes in

Precipitation (GNIP) data set (IAEA/WMO 2014) was used to define the LMWLs, and the relationship between air temperature and $\delta^{18}O$ in precipitation for the six GNIP sites in the QEI (Alert, Eureka, Resolute, Pond Inlet, Mould Bay, and Hall Beach). The six sites contain monthly composite measurements for the 1989–1993 period that were isotopically weighted by the amount of each precipitation event.

Deuterium excess (d) provides an insight into atmospheric humidity and moisture sources and is calculated from (Dansgaard, 1964):

$$d = \delta D - 8\delta^{18}O \quad (2)$$

From eq. (1), the d of the GMWL is +10‰, which indicates that on a global scale, kinetic evaporation of water vapour from oceanic waters is occurring (Merlivat and Coantic 1975). In regions that receive mainly one type of precipitation, such as snow in the QEI, d can provide insight into changing evaporative conditions at the moisture sources (i.e., temperature and relative humidity), or changes in the location of moisture sources (Merlivat and Jouzel 1979; Jouzel et al. 1982).

Snow sampling

In late April and early May 2014, a total of 80 snow samples were collected from four ice caps (Agassiz, Meighen, Devon, and South Melville ice caps) and two glaciers (White and Grise Fiord glaciers) in the QEI (Table 1). These samples represent snow that accumulated between fall 2013 and spring 2014. Sample locations were chosen based on logistical access and broad spatial coverage, to enable investigation of the effects of distance to moisture source and elevation gradients across the study area. Using a similar methodology to Koerner (1979) and Koerner and Russell (1979), snow samples of ~1–2 L volume were collected by inserting a metal pipe (internal diameter ~10 cm), or digging a snow pit, between the snow surface and the last summer surface. The snow samples were transferred to sealed plastic bags in the field, melted, and then a subset was transferred into 30 mL high-density polyethylene (HDPE) scintillation vials without headspace, and returned to the University of Ottawa, Ottawa, Ontario, Canada, for $\delta^{18}O$ and δD analysis. It is assumed that samples provide an average of the entire winter snowpack given the field sampling protocol and melting and mixing of the entire sample prior to transfer to the scintillation vials. All snow samples were collected in air temperatures of <–10 °C, and no above-freezing temperatures had been experienced in 2014 prior to field collection. It is assumed that no sublimation occurred after sample collection due to the retention of samples in sealed plastic bags immediately after collection and melting shortly thereafter.

Ice cores

In April 2009, a 16 m ice core was collected with a Kovacs Mark II corer on Agassiz Ice Cap (A09; 80°49.00′N; 72°53.74′W; 1610 m a.s.l.; Fig. 1), between sites previously cored in 1984 and 1987 (Fisher and Koerner 1988, 1994). This core was shipped frozen to the University of Ottawa, where it was sliced into 2 cm sections in a −20 °C cold room. Each section was melted, then transferred into 30 mL HDPE scintillation vials without headspace. The age–depth time-scale for the A09 core was based on snow stratigraphy, the local precipitation rate and ion chemistry, and confirmed with the Pu isotope peak as radioactive age control as shown by Fisher et al. (2012). The age–depth curve (±2 year error) was used to calculate annual $\delta^{18}O$ averages for the 1938–2009 period (Lecavalier et al. 2017).

In April 2014, a 10 m ice core was collected near the summit of White Glacier (WG14; 79°31.80′N; 91°01.80′W; 1528 m a.s.l.; Fig. 1). This core was cut into 10 cm sections in the field, melted in air-tight bags, and transferred into 30 mL HDPE scintillation vials without headspace prior to shipping. The age–depth time-scale for the WG14 core was established based

Table 1. Information for the 80 snow samples collected for this study in spring 2014.

Latitude (°N)	Longitude (°W)	Elevation (m a.s.l.)	Sample date	$\delta^{18}O$ (‰ VSMOW)	δD (‰ VSMOW)
White Glacier					
79.432	−90.651	53	29 April 2014	−30.3	−231.3
79.435	−90.645	123	29 April 2014	−34.4	−263.1
79.439	−90.648	197	28 April 2014	−34.3	−263.1
79.445	−90.661	234	28 April 2014	−33.6	−255.8
79.446	−90.672	278	28 April 2014	−33.2	−249.0
79.448	−90.685	318	28 April 2014	−29.9	−227.2
79.456	−90.702	363	28 April 2014	−34.8	−266.5
79.456	−90.711	407	28 April 2014	−31.9	−241.9
79.461	−90.743	452	28 April 2014	−33.7	−255.9
79.464	−90.756	504	28 April 2014	−34.1	−248.6
79.476	−90.762	622	28 April 2014	−32.6	−241.8
79.480	−90.771	664	28 April 2014	−34.0	−245.6
79.486	−90.786	714	28 April 2014	−32.2	−233.3
79.489	−90.792	757	28 April 2014	−31.2	−223.0
79.492	−90.796	799	28 April 2014	−36.1	−263.2
79.495	−90.811	842	28 April 2014	−29.7	−212.6
79.499	−90.827	890	28 April 2014	−31.8	−225.8
79.501	−90.837	934	28 April 2014	−30.2	−225.4
79.504	−90.845	982	28 April 2014	−30.3	−226.8
79.507	−90.854	1025	28 April 2014	−27.9	−209.3
79.509	−90.863	1072	28 April 2014	−33.9	−248.7
79.512	−90.876	1118	28 April 2014	−29.4	−218.9
79.515	−90.895	1168	28 April 2014	−32.9	−242.2
79.519	−90.919	1225	28 April 2014	−28.8	−209.9
79.521	−90.942	1255	26 April 2014	−31.0	−225.7
79.525	−90.964	1304	26 April 2014	−32.9	−238.0
79.527	−90.977	1353	26 April 2014	−30.8	−224.6
79.530	−90.999	1401	26 April 2014	−32.2	−236.9
79.534	−90.994	1453	26 April 2014	−31.4	−231.8
79.538	−90.990	1513	26 April 2014	−30.6	−224.4
			Mean ± StDev	−32.0 ± 2.0	−237.0 ± 16.4
Meighen Ice Cap					
79.960	−99.167	235	16 April 2014	−22.6	−167.0
79.935	−99.162	235	16 April 2014	−22.9	−167.5
79.939	−99.073	230	16 April 2014	−25.2	−181.9
79.973	−99.140	222	16 April 2014	−25.4	−183.1
79.977	−99.235	182	16 April 2014	−25.3	−186.0
79.980	−99.100	176	16 April 2014	−27.1	−195.3
79.962	−99.210	168	16 April 2014	−25.4	−184.9
80.000	−99.103	182	16 April 2014	−23.9	−176.1
80.006	−99.312	119	16 April 2014	−26.5	−196.1
80.019	−99.158	136	16 April 2014	−27.2	−202.5
79.919	−99.107	210	16 April 2014	−24.4	−182.4
79.962	−99.059	163	16 April 2014	−26.1	−193.6
			Mean ± StDev	−25.2 ± 1.5	−184.7 ± 11.0
Agassiz Ice Cap					
80.734	−72.881	1739	10 April 2014	−29.6	−228.7
80.745	−72.880	1744	10 April 2014	−33.7	−254.2
80.755	−72.878	1758	10 April 2014	−38.0	−288.2
80.770	−72.874	1758	10 April 2014	−33.1	−252.3
80.780	−72.875	1732	10 April 2014	−37.9	−288.3
80.791	−72.876	1684	10 April 2014	−35.6	−271.7
80.808	−72.327	1498	11 April 2014	−35.6	−271.2
80.878	−71.140	671	11 April 2014	−31.0	−234.6
80.868	−71.293	875	11 April 2014	−32.6	−245.8
80.859	−71.421	998	11 April 2014	−32.9	−248.2
80.851	−71.553	1159	11 April 2014	−31.3	−234.8
80.832	−71.909	1315	11 April 2014	−27.8	−207.3
			Mean ± StDev	−33.3 ± 3.1	−252.1 ± 24.5

Table 1. (*concluded*).

Latitude (°N)	Longitude (°W)	Elevation (m a.s.l.)	Sample date	$\delta^{18}O$ (‰ VSMOW)	δD (‰ VSMOW)
South Melville Ice Cap					
75.393	−114.941	546	22 April 2014	−25.5	−185.3
75.422	−115.010	621	22 April 2014	−24.6	−178.9
75.422	−114.966	642	22 April 2014	−24.5	−176.8
75.426	−115.003	639	22 April 2014	−21.5	−156.3
75.461	−114.995	727	22 April 2014	−29.5	−212.2
75.435	−114.970	664	22 April 2014	−24.2	−172.7
75.455	−114.944	729	22 April 2014	−22.9	−165.8
75.450	−114.933	718	22 April 2014	−23.4	−168.6
			Mean ± StDev	−24.5 ± 2.3	−177.1 ± 16.7
Grise Fiord Glacier					
76.413	−82.721	644	28 April 2014	−23.9	−171.9
76.419	−82.706	592	28 April 2014	−25.5	−183.7
76.421	−82.687	488	28 April 2014	−23.6	−170.0
76.407	−82.744	371	28 April 2014	−28.6	−208.2
			Mean ± StDev	−25.4 ± 2.3	−183.5 ± 17.6
Devon Ice Cap					
75.698	−83.232	274	08 May 2014	−30.5	−229.5
75.671	−83.258	366	08 May 2014	−24.4	−182.1
75.566	−83.154	730	08 May 2014	−25.6	−191.4
75.533	−83.162	1130	08 May 2014	−28.4	−211.6
75.525	−83.196	1172	08 May 2014	−28.7	−214.2
75.723	−83.179	205	08 May 2014	−23.6	−175.3
75.517	−83.433	1175	07 May 2014	−28.7	−212.6
75.526	−83.471	1152	07 May 2014	−26.1	−195.1
75.558	−83.593	974	07 May 2014	−26.5	−197.1
75.492	−83.308	1317	07 May 2014	−27.3	−204.6
75.369	−82.670	1781	07 May 2014	−32.0	−239.2
75.386	−82.763	1731	07 May 2014	−33.6	−252.3
75.404	−82.855	1669	07 May 2014	−31.1	−231.2
75.450	−83.089	1470	07 May 2014	−32.2	−238.8
			Mean ± StDev	−28.5 ± 3.1	−212.5 ± 23.2

Note: VSMOW, Vienna Standard Mean Ocean Water.

on the 1984–2014 mass balance record at stake CJA1, adjacent to the coring location, and the glacier-wide mass balance record from 1960 to 2013 (Thomson et al. 2017), which were converted into a thickness based on the ice or firn composition of the core. This conversion assumed a density of 0.9 g cm^{-3} for ice layers and 0.7 g cm^{-3} for firn layers. Based on this age–depth time-scale, the WG14 core provides annual $\delta^{18}O$ averages for the 1976–2014 period. Air temperatures were well below freezing (typically <–10 °C) during collection of both the A09 and WG14 cores.

δD–$\delta^{18}O$ analysis

The $^{18}O/^{16}O$ and D/H ratios of the snow and ice core samples were determined using a Los Gatos triple isotope water analyzer at the Ján Veizer (formerly G.G. Hatch) Stable Isotope Laboratory, University of Ottawa. The results are presented using the δ-notation ($\delta^{18}O$ and δD), where δ represents the parts per thousand differences for $^{18}O/^{16}O$ or D/H, respectively, in a sample with respect to Vienna Standard Mean Ocean Water. Analytical reproducibility for $\delta^{18}O$ and δD is ±0.1‰ and ±0.3‰, respectively. From the δD–$\delta^{18}O$ measurement, the d was also calculated for the snow and ice samples from eq. (2).

The zonal water isotope model

The global semi-empirical zonally averaged water isotope model has been previously used to simulate $\delta^{18}O$ and δD in polar situations (Fisher 1990, 1991, 1992; Kavanaugh and

Cuffey 2003). The papers of Fisher (1990, 1991, 1992) describe the model's full development and application in a wide range of cases, and a well-illustrated summary of the model, its uses, and key examples of its output appears in Fisher et al. (2004). For the modern situation, the model inputs multi-latitude sources and uses measured zonal annual averages of major water cycle variables such as evaporation rate, total meridional vapour flux, precipitable water content, precipitation, ocean temperature, wind speed, relative humidity, and location of the sea ice front. Figure 5 of Fisher et al. (2004) shows the input fields used to model the 1950–1980 annual global water cycle isotopes and precipitation rates at sea level.

The survival distance for water vapour describes the distance that a slug of source water travels north or south before losing 63% ($1/e$) of its mass by precipitation. The survival time at a given point in the water cycle is measured by the total water content divided by the precipitation rate. The survival distance is then obtained by multiplying this time by the average meridional velocity of the water vapour (total vapour flux/total water content). The values and sources of data are provided by Fisher (1990) and Fisher et al. (2004), with atmospheric data for the 1950–1980 normal period coming from Peixóto and Oort (1983). Fisher (1990, 1992) and Fisher et al. (2004, their figs. 6 and 7) reported that this model successfully simulates zonal annual average sea level $\delta^{18}O$ and d values, as well as the precipitation rate.

The global model provides the initial values for a regional model that starts at the coast and assumes that moisture flux over land has a known trajectory (assumed to be perpendicular to precipitation rate isopleths) from the coast to a given site. The regional model is also empirically driven and requires precipitation, elevation, and air temperature along the trajectory from the coast to the inland sites. A key element of the regional model is the weighting given to moisture sources depending on the elevation of the site, with higher sites receiving less local water. The weighting factor used in the model preserves the vertical profile for total precipitable water and simulates the need for a certain horizontal fetch (L_x = 2700 km for the northern hemisphere), to get moisture from a given ocean source up to the site's elevation (Fisher 1990; Fisher et al. 2004).

To explore the causes of the change in $\delta^{18}O$ and d between the 1970s and 2010s recorded in the ice cores and snow samples, we used the Fisher (1990, 1992) zonal average water isotope model to assess the effect of the individual and combined effects of temperature, vapour flux, and changes in sea ice extent on the values of $\delta^{18}O$ and d in precipitation. Three scenarios were modelled as a function of distance from the Baffin Bay and Arctic Ocean moisture sources along the trajectory line shown in Fig. 1:

(i) $\delta^{18}O$ using the 1950–1980 climate normal.
(ii) $\delta^{18}O$ with a QEI regional air temperature increase of 2.2 °C, an overall northern hemisphere temperature increase of 1 °C, and sea ice 3° farther north, compared with the 1950–1980 climate normal.
(iii) Same as scenario (ii), but with an enhanced meridional vapour flux of 7% compared with the 1950–1980 climate normal.

The mean temperature increase in the QEI of 2.2 °C is based on changes recorded at the five climate stations within and adjacent to the study area (Fig. 2). The northern hemisphere mean temperature increase of 1 °C follows the numbers provided by Hansen et al. (2010). The movement of the sea ice front 3° farther north follows changes in late summer sea ice area between the late 1970s and 2010s tabulated by the National Snow and Ice Data Center (https://nsidc.org/arcticseaicenews/charctic-interactive-sea-ice-graph/), and the study of Serreze and Stroeve (2015). The 7% increase in meridional vapour flux is derived from the increase in average saturated water vapour content in the lower troposphere in the subtropics and temperate zone (the main source region for the QEI) if the average temperature

Fig. 3. (A) Mean monthly δD–$\delta^{18}O$ composition of precipitation at the six Global Network for Isotopes in Precipitation (GNIP) sites in the Queen Elizabeth Islands from 1989 to 1993; (B) δD–$\delta^{18}O$ composition of the 2013–2014 snow samples collected at the six sites in this study (see Fig. 1 for locations); (C) relationship between monthly $\delta^{18}O$ composition of precipitation and mean monthly air temperature at the six GNIP sites from 1989 to 1993; (D) relationship between monthly d in precipitation and mean monthly air temperature at the six GNIP sites from 1989 to 1993. GNIP data set from IAEA/WMO (2014). VSMOW, Vienna Standard Mean Ocean Water.

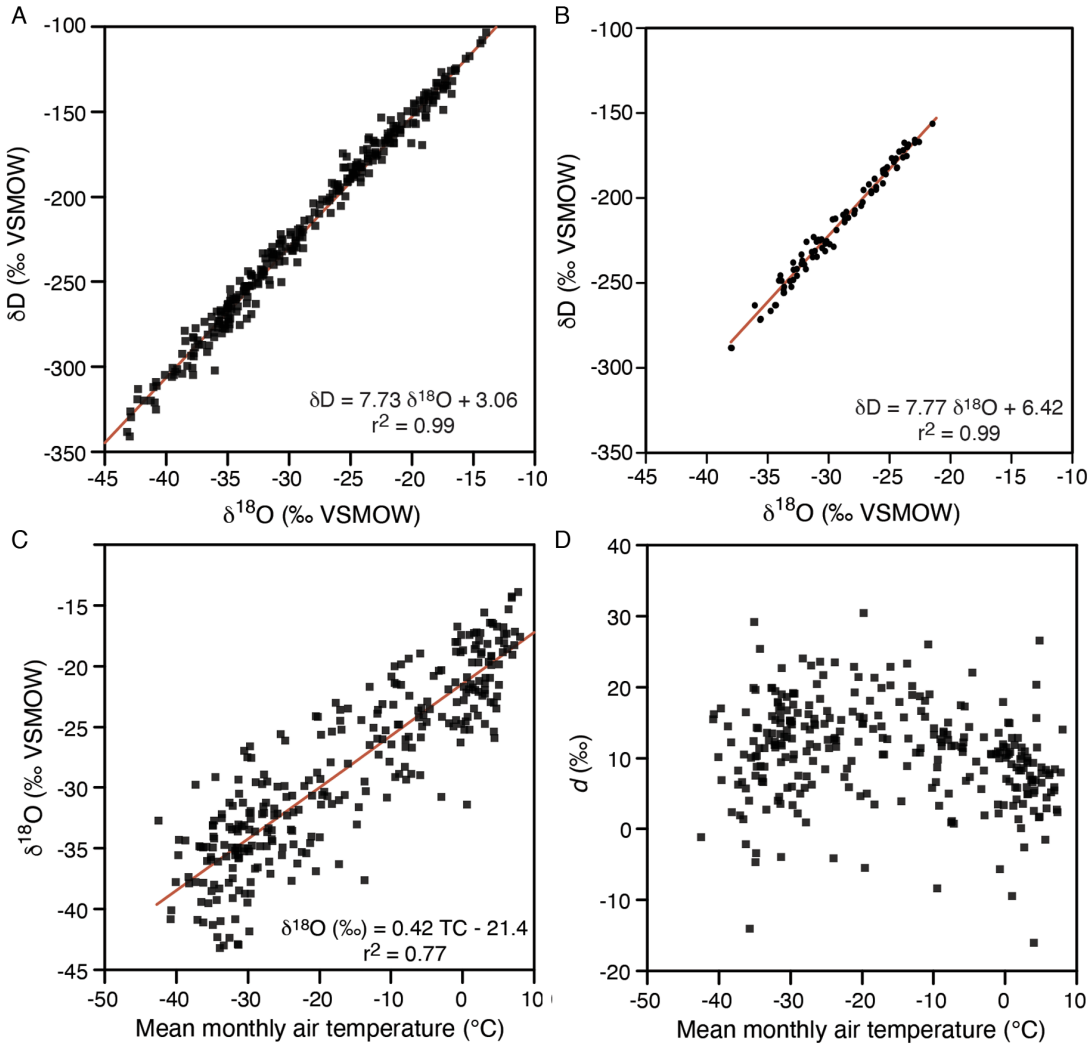

is increased by 1 °C; the zonally averaged precipitation would have to increase by a similar amount, which is within the recorded increase in precipitation in the QEI over the study period of 2.5%–10% (Fig. 2B; Lesins et al. 2010).

Results

The 1989–1993 water isotope composition of precipitation

Precipitation at the six GNIP sites over the period 1989–1993 had mean monthly $\delta^{18}O$ values that ranged from −30.5 ±7.2‰ (Eureka) to −25.8 ±8.0‰ (Mould Bay). The δD–$\delta^{18}O$ composition of precipitation at the six sites (Fig. 3A) plots along a mean regression slope

of 7.73 ($\delta D = 7.73\ \delta^{18}O + 3.06$; $r^2 = 0.99$), with individual LMWLs ranging from 7.29 (Mould Bay) to 8.02 (Pond Inlet) (see table 1 in Lacelle 2011). The values of the slope (7.73) and the *y*-intercept (3.06) are lower than that of the GMWL ($\delta D = 8\ \delta^{18}O + 10$; Craig 1961) due to differences in source water and rainout along moisture trajectories from source. The δD–$\delta^{18}O$ composition of our 2013–2014 snow samples (Fig. 3B) plot along a slope of 7.77, similar to the GMWL and mean LMWL at the GNIP sites, which provides confidence that they did not undergo any significant sublimation, and therefore fractionation, between field collection and analysis.

The monthly $\delta^{18}O$ composition of precipitation at the six GNIP sites is significantly correlated with air temperature ($\delta^{18}O = 0.42 \pm 0.01‰\ °C^{-1} - 21.4‰$; $r^2 = 0.77$; $p < 0.001$; Fig. 3C). This slope is lower than the one calculated by Dansgaard (1964) from sites on the Greenland and Antarctic ice sheets ($\delta^{18}O = 0.69‰\ °C^{-1} - 13.6‰$), but it is consistent with the more recent $\delta^{18}O$-temperature relationship established from borehole temperature profiles from GRIP, NGRIP, Dye-3, and Camp Century in Greenland (0.48‰ $°C^{-1}$; Dahl-Jensen and Johnsen 1986; Dahl-Jensen et al. 1998; Johnsen and Dansgaard 1992; Lecavalier et al. 2013).

The monthly *d* in precipitation at the six GNIP sites in the QEI shows a wide range, varying from –15‰ to +30‰ and displays a small, but insignificant, seasonal trend (Fig. 3D). Winter precipitation tends to have higher *d* due to kinetic fractionation specific to formation of snow (e.g., Edwards et al. 2004). The zonal water isotope model successfully generates this seasonal difference in *d* (Fisher et al. 1990), which provides confidence that it is producing realistic outputs.

The 2013–2014 water isotope composition of snow

The snow that accumulated between fall 2013 and spring 2014 shows a range of $\delta^{18}O$ values that varied across the QEI (Figs. 1 and 4; Table 1). The lowest $\delta^{18}O$ value of −38.0‰ was found near the summit of Agassiz Ice Cap at an elevation of 1758 m a.s.l. Low $\delta^{18}O$ values (near −34.0‰) were also found near the terminus of White Glacier and summit of Devon Ice Cap. Relatively high $\delta^{18}O$ values (near −23‰) were found on Grise Fiord Glacier and Meighen and South Melville ice caps, with the highest value of −21.5‰ found on South Melville Ice Cap at an elevation of 639 m a.s.l.

Figure 5 shows the $\delta^{18}O$-elevation profiles for the 2013–2014 snow samples at each site. Devon Ice Cap showed a significant negative relationship with elevation ($p = 0.01$), with a gradient of $-0.428 \pm 0.001‰\ 100\ m^{-1}$. Three out of the six sites (Agassiz and Melville ice caps, Grise Fiord Glacier) showed a non-significant relationship with elevation ($-0.35‰\ 100\ m^{-1}$, $-0.36‰\ 100\ m^{-1}$, and $1.34‰\ 100\ m^{-1}$, respectively). However, White Glacier and Meighen Ice Cap showed a significant positive relationship with elevation (0.18‰ ± 0.079‰ and 2.83‰ ± 0.81‰ $100\ m^{-1}$, respectively; $p < 0.05$).

In terms of regional patterns (Figs. 1 and 6), there is a statistically significant decrease in average $\delta^{18}O$ values of snow with increasing distance from the coast of Baffin Bay, up to a distance of ~350 km (central Ellesmere Island). For that section of the transect, linear regression analysis of average $\delta^{18}O$ composition of snow versus distance fits the equation $\delta^{18}O = -0.0222x - 25.3$ ($r^2 = 0.73$, $p = 0.10$), where *x* is distance in km. Beyond that distance, towards Axel Heiberg Island, the $\delta^{18}O$ values of snow increase towards the Arctic Ocean to reach maximum values at Meighen Ice Cap.

The 1940–2014 water isotope composition in ice cores

Figure 7 shows the yearly average $\delta^{18}O$ and *d* records from the A09 and WG14 ice cores. The yearly $\delta^{18}O$ average of A09 overlaps well with the previous $\delta^{18}O$ records and age–depth

Fig. 4. $\delta^{18}O$ values of each snow sample location on (A) Meighen Ice Cap, (B) White Glacier, (C) South Melville Ice Cap, (D) Grise Fiord Glacier, (E) Agassiz Ice Cap, and (F) Devon Ice Cap. See Fig. 1 for location of each ice mass. Base imagery: Landsat 8, August and September 2014, courtesy of USGS/NASA Landsat.

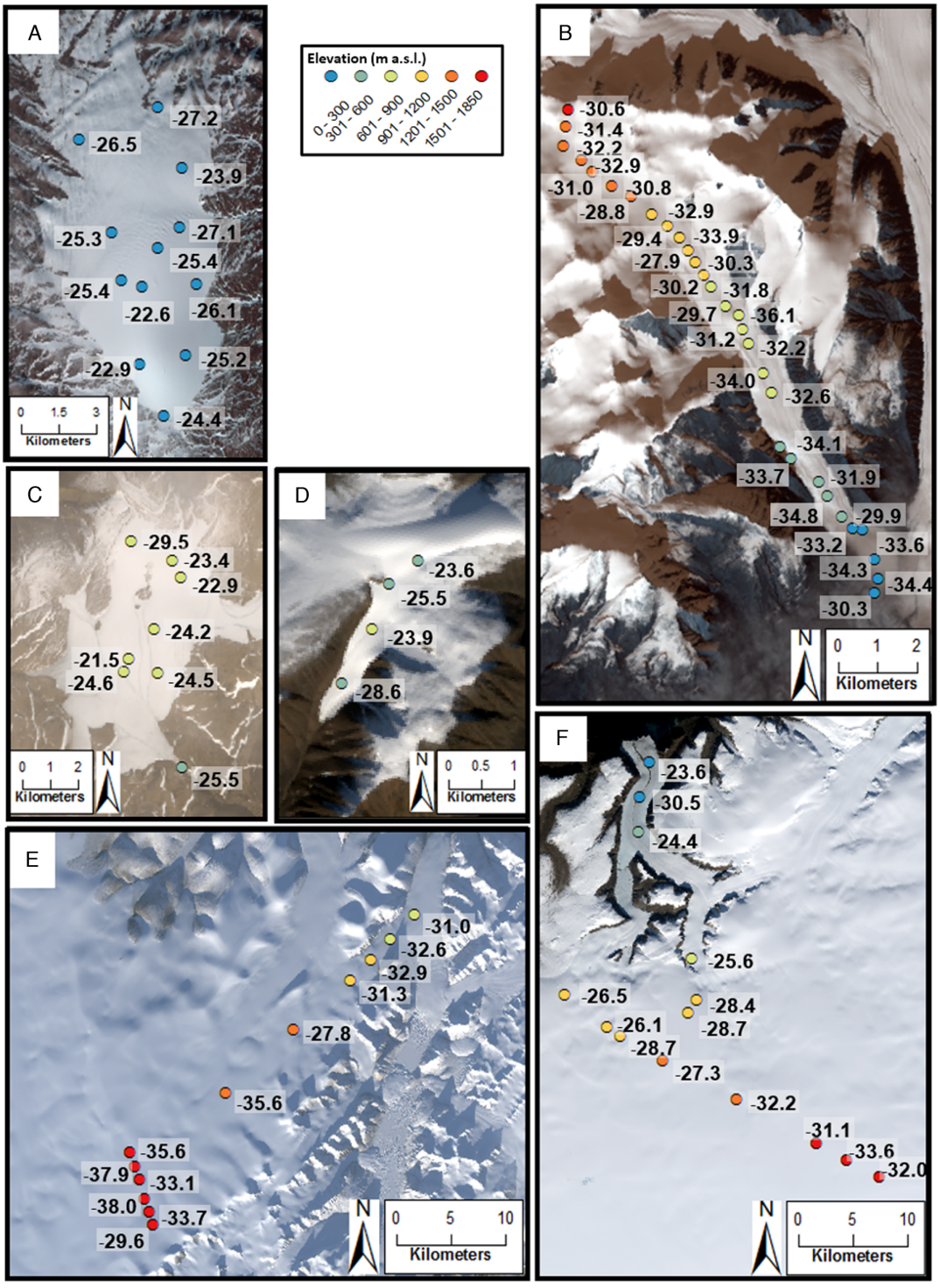

Fig. 5. δ^{18}O-elevation values from the snow sample locations with (A) positive 2013–2014 relationships, (B) negative 2013–2014 relationships. Black best-fit lines are shown for significant relationships. WG, White Glacier; GFG, Grise Fiord Glacier; MeiC, Meighen Ice Cap; AIC, Agassiz Ice Cap; DIC, Devon Ice Cap; MelC, Melville Ice Cap (see Figs. 1 and 4 for locations). For comparison, the δ^{18}O-elevation relationships for the 1973–1974 snow samples measured by Koerner (1979) in similar locations are shown with dashed light grey lines (1 = Sydkap, near Grise Fiord Glacier; 6 and 8 = Agassiz Ice Cap; 10 and 11 = Axel Heiberg Island, near White Glacier; see figs. 1 and 6 of Koerner 1979 for details). VSMOW, Vienna Standard Mean Ocean Water.

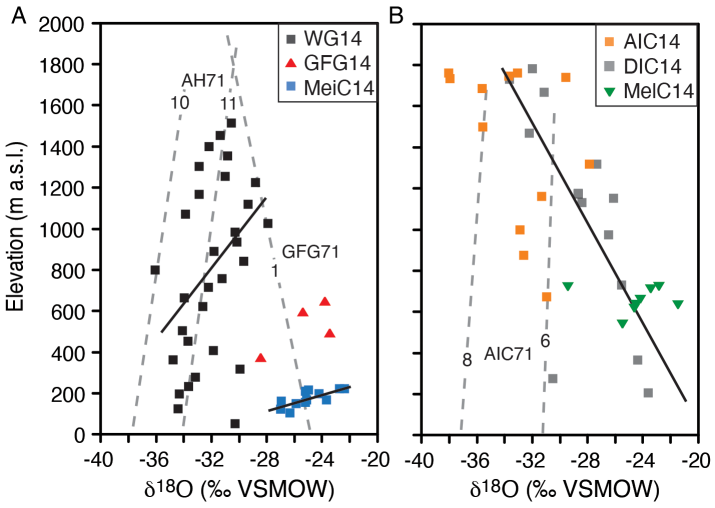

timescales from ice cores A84 and A87 at Agassiz (Fisher and Koerner 1994; Fisher et al. 2012; Lecavalier et al. 2017), providing confidence that the A09 site can be used to extend the historical Agassiz δ^{18}O record to 2009. The 1940–2009 yearly average δ^{18}O record from A09 showed that the highest δ^{18}O value was reached in the late 2000s, whereas the minimum δ^{18}O value was observed in late 1940s (Fig. 7A). The 1976–2014 δ^{18}O record from WG14 ranged from −34.2‰ to −23.1‰, with a generally good fit with the A09 record (Fig. 7A). Overall, the A09 δ^{18}O record showed an increase of 2‰–3‰ from 1940 to 2009, whereas the WG14 δ^{18}O record showed an increase of ~3‰ between 1976 and 2014. A Mann–Kendall test shows that the δ^{18}O increase at WG14 is statistically significant ($p = 0.05$) over the period 1976–2014; the increase at A09 is not statistically significant over the period 1940–2009, although this is sensitive to the period analyzed. Note that the unusually low δ^{18}O WG14 value of −34.2‰ recorded in 2013 reflects anomalously cold conditions that year, with summer 2013 mean air temperatures up to 2.5 °C below the 1981–2010 mean (Sharp et al. 2015; Thomson et al. 2017).

The *d* records from A09 and WG14 are shown in Fig. 7B. The A09 time-series has *d* values ranging from −12.3‰ to 14.8‰, with *d* being mostly above 0‰ for the pre-1970 period. Despite showing similar δ^{18}O time-series, the WG14 time-series has much higher *d* values than A09, ranging from 6.1‰ to 35.4‰. However, both A09 and WG14 show a generally decreasing trend of 5‰–7‰ in *d* values towards the present day. A Mann–Kendall test shows a significant decrease in the values of *d* in the A09 core ($p = 0.05$), at an average rate of −0.064‰ yr^{-1} over the period 1940–2009. In the WG14 core, the decrease in *d* is more significant ($p = 0.001$), at a rate of −0.233‰ yr^{-1} over the period 1976–2014, although this rate is biased by the anomalously high *d* values in 1983–1984 (Fig. 7B).

Fig. 6. Comparison of (A) average snow $\delta^{18}O$ and (B) *d* composition, in 1973–1974 (black x-markers) and 2013–2014 (black squares) with predicted values from a zonal average water isotope model. Regional average solutions were produced as a function of distance from moisture sources along the trajectory shown in Fig. 1 (Fisher 1990). The standard deviation of the average $\delta^{18}O$ composition ranges from 1.5‰ to 2.5‰ for each site (not shown due to *y*-axis scale). The change in $\delta^{18}O$ and *d* of precipitation in the Queen Elizabeth Islands (QEI) since the 1970s can be best explained by scenario iii (red dots), which includes the enhanced meridional vapour flux and wetter climate. (C) Accumulation rate relative to distance from the respective coast. Mei IC, Meighen Ice Cap; Mel IC, Melville Ice Cap; WG, White Glacier; AIC, Agassiz Ice Cap; DIC, Devon Ice Cap; GFG, Grise Fiord Glacier; VSMOW, Vienna Standard Mean Ocean Water.

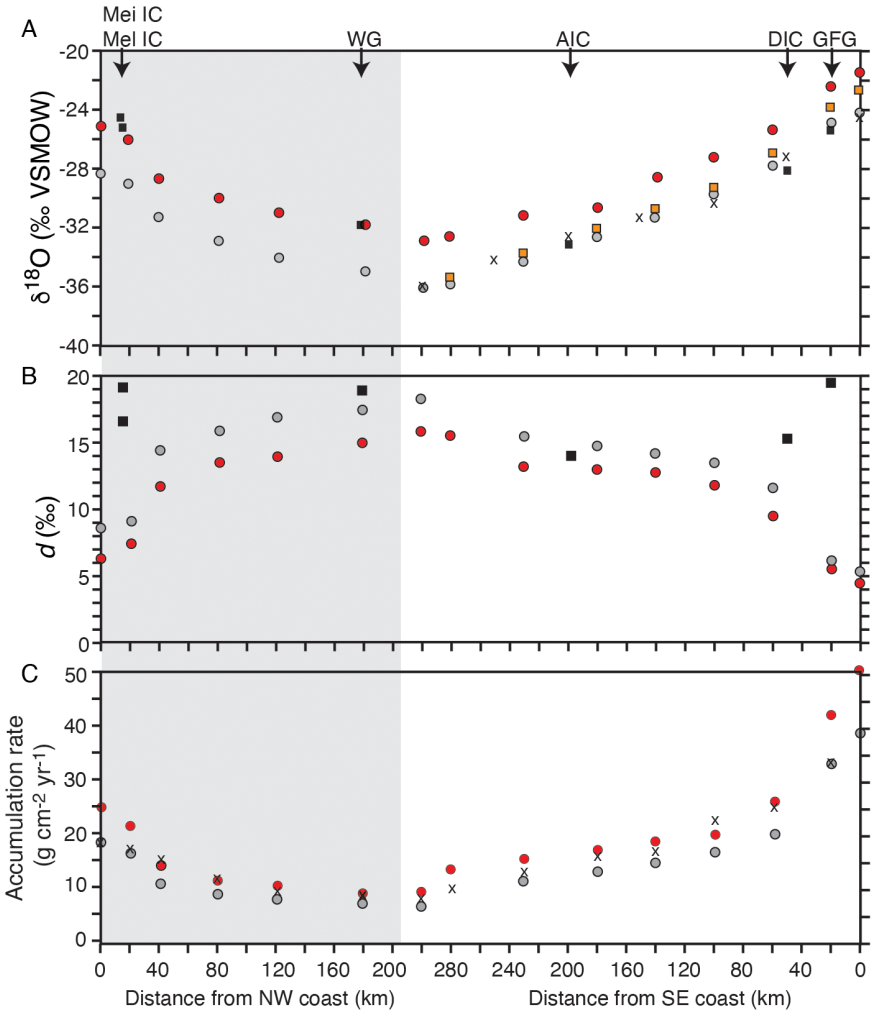

Measurements:
x 1973-74 average snow $\delta^{18}O$ along vapor trajectory shown in Fisher (1990).
■ 2014 average snow $\delta^{18}O$.

Modeling scenarios:
● i. $\delta^{18}O$ along vapor trajectory using 1950-80 climate normal (Fisher, 1990).

■ ii. $\delta^{18}O$ along vapor trajectory using: 1) QEI regional air temperature increased by 2.2°C; 2) North hemisphere temperature increased by 1°C; 3) sea ice 3° farther north.

● iii. $\delta^{18}O$ along vapor trajectory using: 1) QEI regional air temperature increased by 2.2°C; 2) North hemisphere temperature increased by 1°C; 3) sea ice 3° farther north; 4) enhanced meridional flux by 7%.

Fig. 7. (A) $\delta^{18}O$ and (B) *d* time-series of Agassiz Ice Cap (A09) and White Glacier (WG14) ice core records. Shown for comparison are the Agassiz Ice Cap A84 and A87 ice core $\delta^{18}O$ records from Lecavalier et al. (2017).

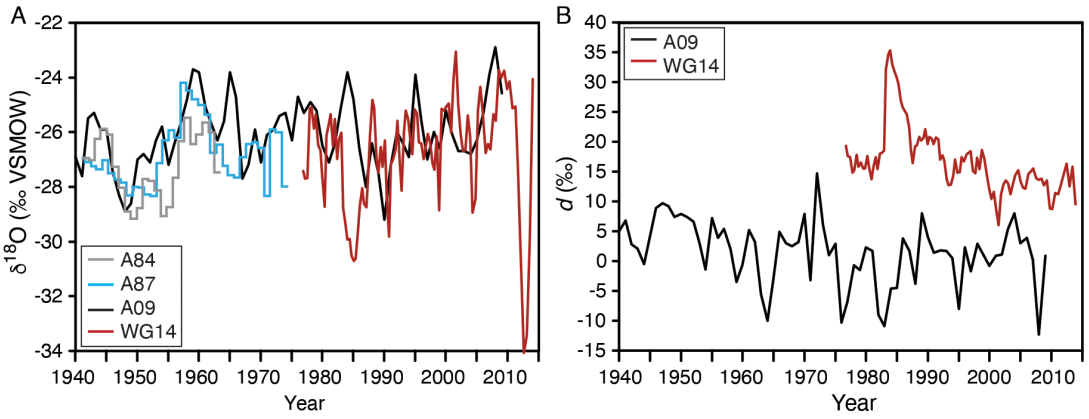

Discussion

Changes in regional patterns of $\delta^{18}O$ of snow

The precipitation in the study region moves mainly from the Baffin Bay area along a north–northwest gradient across the QEI, with the condensation process being twofold: orographic precipitation along the eastern slopes (i.e., adiabatic cooling of uplifting of air mass) and isobaric cooling in the interior (i.e., rainout at constant condensation altitude). Koerner and Russell (1979) found that ~26% of precipitation at sea level on southeast Devon Island originates from Baffin Bay, but at high elevation this value was down to ~8% as moisture is sourced from much farther away. The Arctic Ocean is another, but less significant moisture source in the region, mainly affecting the western coastal areas. The moisture source and processes driving precipitation in the QEI should be reflected in the $\delta^{18}O$ and *d* composition of precipitation.

Figure 1 compares the 2013–2014 average $\delta^{18}O$ values in the snow transects with the 1973–1974 snow measurements of Koerner (1979). In the western QEI, the 2013–2014 average $\delta^{18}O$ snow composition were approximately 2‰–3‰ higher than in the 1970s, whereas in the eastern QEI, the $\delta^{18}O$ values were similar to those collected by Koerner (1979). The plotted 2014 values are the mean and standard deviation recorded at each sample location, whereas Koerner's values represent the mid-point value along the transect. Before addressing the change in $\delta^{18}O$ composition of precipitation, we first explore if there are changes in $\delta^{18}O$ trends representing changes in processes driving precipitation between 1973–1974 and 2013–2014.

Isobaric cooling and snow $\delta^{18}O$ composition

In both 1973–1974 and 2013–2014, snow $\delta^{18}O$ values exhibited a decreasing trend from Baffin Bay to central Ellesmere Island; beyond that distance, the $\delta^{18}O$ values of snow increased towards Axel Heiberg Island and the Arctic Ocean to reach maximum values at Meighen Ice Cap (Fig. 1). The 1973–1974 and 2013–2014 data sets fit similar linear regression slope values of $\delta^{18}O$ versus distance from northwest Baffin Bay (1971–1973: $\delta^{18}O = -0.0195x - 26.0$; $r^2 = 0.78$; 2013–14: $\delta^{18}O = -0.0222x - 25.3$, $r^2 = 0.73$). Koerner (1979) suggested from the linear regression analysis that ~80% of the precipitation in the interior section of the QEI originated from Baffin Bay, with the $\delta^{18}O$ composition reflecting isobaric cooling towards the interior following the uplift of air masses along the eastern mountain range. The similar regression slope and r^2 obtained in the 2014 snow data set suggests that precipitation

in the southeastern section of the QEI continues to originate from northwest Baffin Bay, with rainout caused by isobaric cooling. This is expected given that the effect of isobaric cooling on $\delta^{18}O$ of snow is a function of distance to moisture source and its Rayleigh fractionation during rainout, a process that should remain largely unchanged over time.

Elevation (adiabatic cooling) and snow $\delta^{18}O$ composition

The $\delta^{18}O$-elevation relationship is largely temperature dependent (Rowley 2007). Globally, a modern slope of about −0.28‰ 100 m^{-1} to −0.33‰ 100 m^{-1} is observed (Rowley 2007; Clark 2015), but a series of shallow ice cores from the Greenland Ice Sheet define the $\delta^{18}O$-elevation relationship of Arctic regions as −0.62‰ ±0.03‰ 100 m^{-1} (Johnsen et al. 1989; Dahl-Jensen et al. 2013). Similar $\delta^{18}O$-elevation slopes of −0.65‰ 100 m^{-1} to −0.64‰ 100 m^{-1} were measured by Koerner (1979) and Koerner and Russell (1979) along the southeast coast of the QEI. However, out of the six elevational transects taken across the QEI in 2014, only the transect on the northwest side of Devon Ice Cap demonstrated a significant decrease of snow $\delta^{18}O$ values with elevation (Fig. 5B). Transects from Agassiz Ice Cap showed a non-significant negative relationship with elevation, whereas those from White Glacier and Meighen Ice Cap (both situated on the western side of the QEI) showed a significant positive relationship with elevation (Fig. 5A).

Our observation in 2014 of a significant negative gradient of −0.43‰ ±0.01‰ 100 m^{-1} ($p = 0.01$) along the northwestern (Sverdrup Glacier) side of Devon Ice Cap, a gradient similar to the expected $\delta^{18}O$-elevation relation, differs from the observations of Koerner (1979) and Koerner and Russell (1979). They found that samples taken on Sverdrup Glacier in 1972 increased in $\delta^{18}O$ value with elevation; however, samples taken along the same transect in 1971 and 1973 showed no significant change with elevation. Koerner and Russell (1979) attributed their patterns to the orographic movement of air across the ice cap summit from the southeast to the northwest in 1972, but that frequent wind scouring and redistribution of snow by wind drift likely disturbed this pattern in 1971 and 1973.

A significant question then is why were the $\delta^{18}O$-elevation patterns observed on the northwest part of Devon Ice Cap in 2014 so different to those observed in the 1970s? An answer can be provided by the study of Wohlleben (2009), who demonstrated that orographic precipitation does in fact occur over the northwest portion of Devon Ice Cap, as northwesterly winds move moisture from Hells Gate polynya up the ice cap. Wohlleben (2009) supported her findings with an analysis of mean tropospheric wind patterns over the period 1975–2000 and the asymmetric cross-profile of Devon Ice Cap, in which the ice cap summit is shifted towards the northwest due to increased precipitation on that side. Temperature measurements on northwestern Devon Ice Cap in 2013–2014 show a general decrease with altitude (Fig. 8), although there was often little difference between temperatures at 1300 and 1800 m a.s.l. elevation, particularly in the fall when most annual snowfall occurs. This supports the fact that orographic uplift is likely the primary driver of the significant decrease in $\delta^{18}O$ with elevation observed on northwestern Devon Ice Cap in 2014, the only location in our study area where a significant inverse relationship was observed. However, local synoptic conditions, including snow drifting (that can move snow with negative $\delta^{18}O$ values from high elevations to low elevations), and riming (that preferentially deposits ice with higher $\delta^{18}O$ values; Demoz et al. 1991), may cause site-specific variations when attempting to compare $\delta^{18}O$ snow composition among sampling years.

Temperature inversions and snow $\delta^{18}O$ composition (equivalent elevation)

The 2014 $\delta^{18}O$ snow transects on White Glacier and Meighen Ice Cap showed significant positive relationships with elevation (Fig. 5A). On White Glacier, the $\delta^{18}O$ values near the

Fig. 8. Five-day running mean temperatures measured at 300, 1300, and 1800 m a.s.l. on the northwestern portion of Devon Ice Cap (Sverdrup Glacier) in 2013–2014.

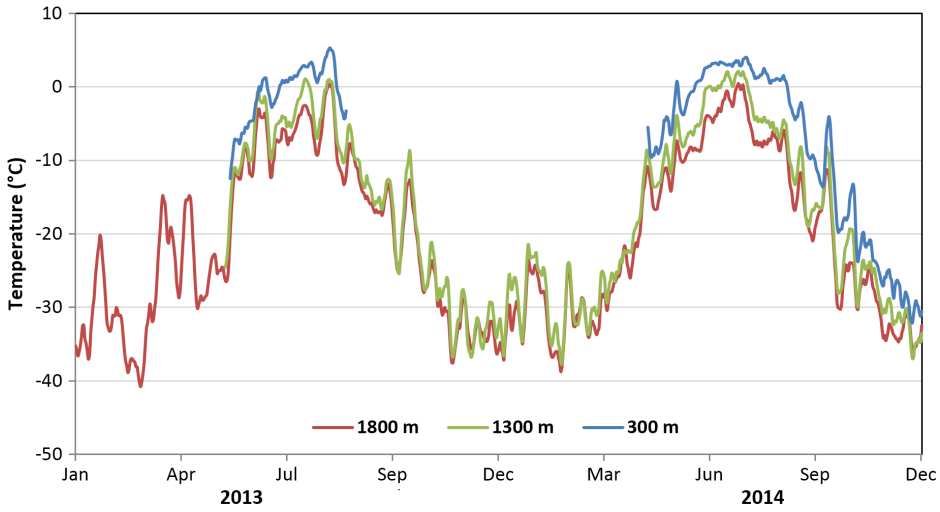

Fig. 9. Five-day running mean temperatures measured in 2012 at the terminus (35 m a.s.l.) and summit nunatak (1511 m a.s.l.) of White Glacier, and at Eureka Climate Station.

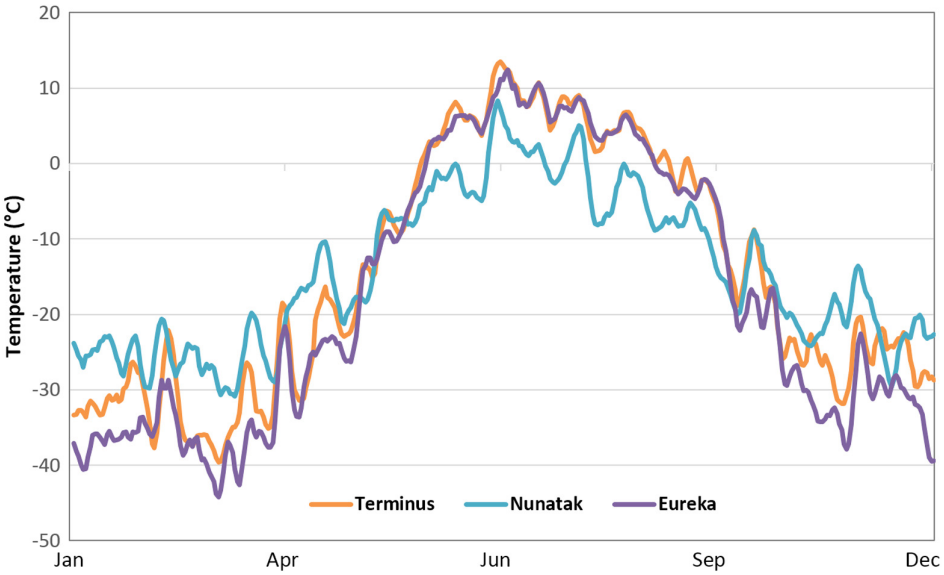

glacier terminus had a wide range (−34.4‰ to −30.3‰); the lowest $\delta^{18}O$ value (−36.1‰) was measured in the center of the glacier at 750 m a.s.l., and above this the $\delta^{18}O$ values mainly increased towards the top of the glacier to reach ~−29‰ (Fig. 4B). To investigate this further, we compared the five-day running mean air temperatures recorded at the glacier terminus (~35 m a.s.l.) and near the glacier summit on a nunatak (~1511 m a.s.l.) (Fig. 9). Temperatures at the terminus are typically higher than at the nunatak in the summer (May to October), but in the winter months (October to May), the temperatures at the

Fig. 10. δ^{18}O-elevation (Z_x, black squares) and δ^{18}O-equivalent elevation (Z'_x, red squares) relationships of 2013–2014 snow samples collected along the centreline of White Glacier. The Z_x values show a positive relationship with elevation due to winter temperature inversions but correcting for this effect results in a negative Z'_x value of −0.49‰ 100 m^{-1} (red line).

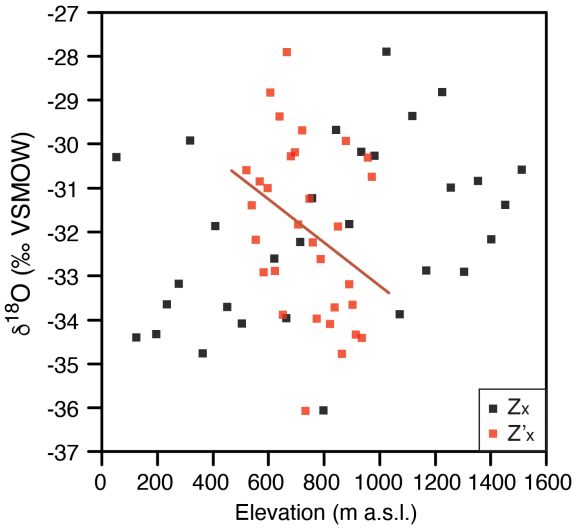

nunatak can reach up to ~10 °C warmer than those observed at the terminus. These strong winter inversions are common on Arctic glaciers and ice caps (Mernild and Liston 2010), and typically occur between January and April when there is a large temperature difference between the land and the surrounding ocean, with limited radiation and anticyclonic conditions (Serreze et al. 1992). This temperature inversion can, therefore, explain the inverted δ^{18}O values on White Glacier. As there are no temperature data available from different elevations on Meighen Ice Cap, we cannot demonstrate that the same winter inversion occurs there. However, Maxwell (1981) discovered that winter surface temperature inversions occur frequently (~80% of the time) along the northwestern portion of the Canadian Arctic Archipelago (CAA).

In mountainous regions, the concept of equivalent elevation was developed to deal with winter temperature inversions below treeline in permafrost modelling (Lewkowicz and Bonnaventure 2011). Equivalent elevation modifies the true elevation to consider weakened or reversed surface lapse rate in the forest compared with the normal surface lapse rate above treeline. Equivalent elevation can be calculated using the following equation (Lewkowicz and Bonnaventure 2011):

$$Z'_x = Z_t - (Z_t - Z_x) \times \frac{L_1}{L_2} \quad (3)$$

where Z'_x is the equivalent elevation, Z_t is the elevation where change in lapse rate occurs, Z_x is the true elevation, L_1 is the lapse rate below treeline, and L_2 is the normal lapse rate above treeline.

The lapse rate terms in eq. (3) were modified to account for the geographical setting of White Glacier, and that we are dealing with δ^{18}O rather than air temperature. In our application, L_1 and L_2 represent the δ^{18}O–elevation relationships above and below the elevation where the change between positive and negative δ^{18}O trends with elevation is observed. On White Glacier, this change occurs near 850 m a.s.l.; below that the δ^{18}O-elevation

relationship is 0.069‰ 100 m^{-1}, and above that it is −0.23‰ 100 m^{-1} ($r^2 = 0.08$ for all data, $p > 0.10$). Using these values for the Z_t, L_1, and L_2 parameters in eq. (3) modifies the elevations of samples collected on the glacier to produce a $\delta^{18}O$-equivalent elevation (Fig. 10). The elevation relationship of the data then becomes −0.49‰ 100 m^{-1} ($r^2 = 0.11$, $p < 0.10$), which is in line with expected values for Arctic regions and significant at the 90% level. This concept of equivalent-elevation can, therefore, provide a solution to locations that experience strong temperature inversions when attempting to produce global to regional distribution maps of $\delta^{18}O$ in precipitation (e.g., Bowen and Wilkinson 2002; Wang et al. 2009).

Temporal change in $\delta^{18}O$-*d* composition of precipitation

The $\delta^{18}O$ values from snow and firn samples are typically representative of air temperature at the time of condensation, source and water vapour history, and snow surface processes, and can, therefore, vary due to factors such as elevation, topography, air temperature, distance from the moisture source, and snow drifting (Beltrami and Taylor 1995). Of these effects, elevation, distance from the moisture source, and air temperature have previously been found to be the dominant controlling factors in the QEI (Fisher 1990). However, comparison of snow $\delta^{18}O$ composition between years can be made challenging by local synoptic conditions (e.g., drifting and riming) that can exert dominant controls on the snow sample $\delta^{18}O$ values, as discussed in the section "Elevation (adiabatic cooling) and snow $\delta^{18}O$ composition" for Devon Ice Cap.

In ice cores, these effects are minimized when $\delta^{18}O$ trends are explored at multi-annual resolution (Fisher et al. 1985; Fisher and Koerner 1994). The 1975–2014 $\delta^{18}O$ and *d* time-series from the Agassiz and White Glacier ice cores are similar for their overlapping periods (Fig. 7), with both showing a 2‰–3‰ increase in $\delta^{18}O$ and 5‰–7‰ decrease in *d* over time. The snow $\delta^{18}O$ composition between 1973–1974 and 2013–2014 showed a similar increase for the western section of the QEI, although the eastern QEI had similar values likely due to local synoptic conditions. The $\delta^{18}O$-temperature relationship of 0.42‰ $°C^{-1}$ at the six GNIP sites (Fig. 3C) suggests that a temperature warming of 2–4 °C would result in an increase of 0.8‰–1.7‰ in $\delta^{18}O$ values in precipitation, much lower than the observed 2‰–3‰ increase.

The model results for the isotope and accumulation values along the two trajectories shown on the map in Fig. 1 are plotted in Fig. 6, along with the average $\delta^{18}O$ composition of snow in 1973–1974 and 2013–2014 for each site. The northwest trajectory passes close to White Glacier, but the Agassiz ice core site is on a different trajectory. Under scenario (ii) with QEI regional air temperature increase of 2.2 °C, an overall northern hemisphere temperature increase of 1 °C, and sea ice 3° farther north, compared with the 1950–1980 climate normal, the prediction is that the $\delta^{18}O$ of precipitation would increase by <1‰, much lower than the observed increase of 2‰–3‰. From this analysis, it is apparent that changes in local sea ice extent make a contribution to changes in the local water input and precipitation, and its $\delta^{18}O$ value, but this effect is limited to coastal regions; for higher elevation sites moisture originates from much farther way, and changes in sea ice extent have little effect on their $\delta^{18}O$ values in precipitation (i.e., Koerner and Russell 1979; Fisher 1990). However, if we enhance the total meridional vapour flux by 7% in scenario (iii), the $\delta^{18}O$ of precipitation is predicted to increase by 2‰–3‰, with an associated decrease in *d* of about the same order. Therefore, the change in $\delta^{18}O$ and *d* of precipitation in the QEI since the 1970s cannot be attributed solely to warmer temperatures and changes in sea ice extent, but also to the enhanced total meridional vapour flux and wetter climate.

However, it must be remembered that these factors can't be viewed in isolation as, for example, Arctic temperature amplification has been attributed to increased meridional heat transport (Graversen et al. 2008) and loss of the sea ice cover (Serreze et al. 2009),

whereas reduced sea ice extent can be driven by increased meridional vapour flux (i.e., increased storminess) and incursions of warmer ocean water driven by increased air temperatures (Kinnard et al. 2011). It also takes ~2500 km to mix a given isotope source completely into the troposphere (Fisher 1990), and sites closer to sea level are more impacted by these changes than those at high altitude (Koerner and Russell 1979). It is beyond the scope of this study to quantify the complex interactions of these processes across a wide range of scenarios, but it is clear that measured changes in isotopes in the QEI are not solely driven by local changes in air temperature and sea ice.

Conclusions

Interpretation of temporal changes in the isotopic composition of individual snow samples can have high uncertainty due to factors such as wind scouring, snow drifting, riming, and local synoptic conditions, but by comparing 80 samples collected at six sites across the QEI, it is clear that there has been a general increase in $\delta^{18}O$ values and decrease in *d* values over the period from 1973–1974 to 2013–2014. These trends are supported by statistically significant changes in the values of $\delta^{18}O$ and *d* in multi-decadal records from an ice core from White Glacier, and *d* from an ice core at Agassiz Ice Cap. These results highlight the effectiveness of combining a variety of data sources to derive isotopic trends in traditionally noisy data sets (Fisher and Koerner 1994).

The QEI has experienced a 3.2 °C increase in mean annual temperature at Eureka Climate Station over the period 1972–2007 and 10% increase in precipitable water there over the period 1961–2007 (Lesins et al. 2010), similar to average patterns recorded at climate stations across the QEI (Fig. 2; Environment Canada 2015). Based on the present and historical $\delta^{18}O$ composition of snow and ice in the QEI presented in this study, the following conclusions can be reached:

a. Regional temperatures and distance from moisture source provide a dominant control on the spatial patterns in $\delta^{18}O$ values of 2013–2014 snow, with the colder winter air temperatures in the western CAA (−28 °C to −32 °C) and northern CAA (−35 °C to −38 °C) contributing to the lower $\delta^{18}O$ values on White Glacier and Agassiz Ice Cap, respectively (Maxwell 1981). There are two main moisture sources in the CAA: the Arctic Ocean and Baffin Bay. As air masses cool isobarically when they move farther from these moisture sources they deplete the total amount of ^{18}O in the air masses, and, thus, in the snow (Koerner 1979).
b. Temperature inversions contributed to the inverse relationship between $\delta^{18}O$ values and elevation for White Glacier, with winter temperatures up to 10 °C lower at the terminus than at the summit. It is likely that Meighen Ice Cap also undergoes a similar winter inversion as White Glacier, explaining the cause of the inverse relationship of $\delta^{18}O$ with elevation there.
c. $\delta^{18}O$ time-series of ice cores from White Glacier and Agassiz Ice Cap indicate increases of 2‰–3‰ since the 1970s. Modelling suggests that observed increases in air temperature and reductions in sea ice extent cannot explain this change in $\delta^{18}O$ alone, but rather a combination of warmer temperatures and enhanced meridional vapour flux is required, reflective of a warmer–wetter climate in the QEI between the 1970s and 2010s.

Acknowledgements

We wish to thank the Natural Sciences and Engineering Research Council of Canada, Polar Continental Shelf Program, Canada Foundation for Innovation, Ontario Research Fund, Climate Change Geoscience Program (Natural Resources Canada), ArcticNet Network of Centres of Excellence, and University of Ottawa for funding. We thank the Nunavut Research Institute, Aurora Research Institute, and the communities of Sachs

Harbour (NT), Ulukhaktok (NT), Grise Fiord (NU), and Resolute Bay (NU) for permission to conduct research on ice caps and glaciers in the Queen Elizabeth Islands. We would like to thank Alison Cook for assistance with producing Fig. 1, Miles Ecclestone and Chris Omelon for assistance with collecting field samples, Wayne Pollard for logistical support, and the McGill Arctic Research Station for hosting White Glacier field activities.

References

Beltrami, H., and Taylor, A.E. 1995. Records of climatic change in the Canadian Arctic: towards calibrating oxygen isotope data with geothermal data. Glob. Planet. Change, **11**(3): 127–138. doi: 10.1016/0921-8181(95)00006-2.

Bowen, G.J., and Wilkinson, B. 2002. Spatial distribution of $\delta^{18}O$ in meteoric precipitation. Geology, **30**(4): 315–318. doi: 10.1130/009-613(2002)030<0315:SDOOIM>2.0.CO;2.

Box, J.E., Colgan, W.T., Wouters, B., Burgess, D.O., O'Neel, S., Thomson, L.I., and Mernild, S.H. 2018. Global sea-level contribution from Arctic land ice: 1971–2017. Environ. Res. Lett. **13**(12): 125012. doi: 10.1088/1748-9326/aaf2ed.

Clark, I.D. 2015. Groundwater Geochemistry and Isotopes. CRC Press, Taylor & Francis Group, Boca Raton, Fla., USA, 456 pp.

Craig, H. 1961. Isotopic variations in meteoric waters. Science, **133**: 1702–1708. doi: 10.1126/science.133.3465.1702.

Dahl-Jensen, D., and Johnsen, S.J. 1986. Paleotemperatures still exist in the Greenland Ice Sheet. Nature, **320**: 250–252. doi: 10.1038/320250a0.

Dahl-Jensen, D., Mosegaard, K., Gundestrup, N., Clow, G.D., Johnsen, S.J., Hansen, A.W., and Balling, N. 1998. Past temperatures directly from the Greenland Ice Sheet. Science, **282**: 268–271. doi: 10.1126/science.282.5387.268.

Dahl-Jensen, D, Aldahan, A., Albert, M.R., Azuma, N., Balslev-Clausen, D., Baumgartner, M., et al. 2013. Eemian interglacial reconstructed from a Greenland folded ice core. Nature, **493**: 489–494. doi: 10.1038/nature11789.

Dansgaard, W. 1964. Stable isotopes in precipitation. Tellus, **16**: 436–468. doi: 10.3402/tellusa.v16i4.8993.

Demoz, B., Warburton, J., and Stone, R. 1991. The influence of riming on the oxygen isotopic composition of ice-phase precipitation. Atmos. Res. **26**: 463–488. doi: 10.1016/0169-8095(91)90039-Y.

Derksen, C., Smith, S.L., Sharp, M., Brown, L., Howell, S., Copland, L, et al. 2012. Variability and change in the Canadian cryosphere. Clim. Change, **115**(1): 58–88. doi: 10.1007/s10584-012-0470-0.

Edwards, T.W.D., Wolfe, B.B., Gibson, J.J., and Hammarlund, D. 2004. Use of water isotope tracers in high latitude hydrology and paleohydrology. *In* Long-term environmental change in Arctic and Antarctic Lakes. Developments in paleoenvironmental research. *Edited by* J.P. Smol, R. Pienitz, and M.S.V. Douglas. Vol. 8. Springer, Dordrecht, the Netherlands. doi: 10.1007/978-1-4020-2126-8_7.

Environment Canada 2015. Historical Canadian climate database. https://climate.weather.gc.ca/.

Fisher, D.A. 1990. A zonally-averaged stable-isotope model coupled to a regional variable-elevation stable-isotope model. Ann. Glaciol. **14**: 65–71. doi: 10.1017/s0260305500008284.

Fisher, D.A. 1991. Remarks on the deuterium excess in precipitation in cold regions. Tellus B: Chem. Phys. Meteorol. **438**: 401–407. doi: 10.3402/tellusb.v43i5.15414.

Fisher, D.A. 1992. Stable isotope simulations using a regional stable isotope model coupled to a zonally averaged global model. Cold Reg. Sci. Technol. **21**: 61–77. doi: 10.1016/0165-232X(92)90006-G.

Fisher, D.A., and Koerner, R.M. 1988. The effects of wind on $\delta(^{18}O)$ and accumulation give an inferred record of seasonal δ amplitude from the Agassiz Ice Cap, Ellesmere Island, Canada. Ann. Glaciol. **10**: 34–37. doi: 10.3189/S0260305500004122.

Fisher, D.A., and Koerner, R.M. 1994. Signal and noise in four ice-core records from the Agassiz Ice Cap, Ellesmere Island, Canada: details of the last millennium for stable isotopes, melt and solid conductivity. The Holocene, **4**(2): 113–120. doi: 10.1177/095968369400400201.

Fisher, D.A., Reeh, N., and Clausen, H.B. 1985. Stratigraphic noise in time series derived from ice cores. Ann. Glaciol. **7**: 76–83. doi: 10.3189/S0260305500005942.

Fisher, D., Zheng, J., Burgess, D., Zdanowicz, C., Kinnard, C., Sharp, M., and Bourgeois, J. 2012. Recent melt rates of Canadian Arctic ice caps are the highest in many millennia. Glob. Plan. Change, **84–85**: 3–7. doi: 10.1016/j.gloplacha.2011.06.005.

Fisher, D.A., Wake, C., Kreutz, K., Yalcin, K., Steig, E., Mayewski, P., et al. 2004. Stable isotope records from Mount Logan, Eclipse ice cores and nearby Jellybean Lake. Water cycle of the North Pacific over 2000 years and over five vertical kilometres: sudden shifts and tropical connections. Géogr. Phys. Quat., **58**: 337–352, doi: 10.7202/013147ar.

Graversen, R.G., Mauritsen, T., Tjernström, M., Källén, E., and Svensson, G. 2008. Vertical structure of recent Arctic warming. Nature, **451**: 53–56. doi: 10.1038/nature06502.

Hansen, J., Ruedy, R., Sato, M., and Lo, K. 2010. Global surface temperature change. Rev. Geophys. **48**: RG4004. doi: 10.1029/2010RG000345.

Harig, C., and Simons, F.J. 2016. Ice mass loss in Greenland, the Gulf of Alaska, and the Canadian Archipelago: Seasonal cycles and decadal trends. Geophys. Res. Lett. **43**(7): 3150–3159. doi: 10.1002/2016GL067759.

IAEA/WMO (International Atomic Energy Agency/World Meteorological Organization). 2014. Global network of isotopes in precipitation. GNIP Database. https://www.iaea.org/services/networks/gnip.

Jakobsson, M., Mayer, L. A., Coakley, B., Dowdeswell, J. A., Forbes, S., Fridman, B., et al. 2012. The International Bathymetric Chart of the Arctic Ocean (IBCAO) version 3.0. Geophys. Res. Lett. **39**(12): L12609. doi: 10.1029/2012GL052219, PMID: 32647176.

Johnsen, S.J., Dansgaard, W., and White, J.W.C. 1989. The origin of Arctic precipitation under present and glacial conditions. Tellus B, **41**(4): 452–468. doi: 10.3402/tellusb.v41i4.15100.

Johnsen, S.J., and Dansgaard, W. 1992. On flow model dating of stable isotope records from Greenland ice cores. *In* The last deglaciation: Absolute and radiocarbon chronologies. *Edited by* E. Bard and W. S. Broecker. NATO ASI Series I, 2, pp. 13–24.

Jouzel, J., Merlivat, L., and Lorius, C. 1982. Deuterium excess in an east Antarctic ice core suggests higher relative humidity at the oceanic surface during the last glacial maximum. Nature, **299**: 688–691. doi: 10.1038/299688a0.

Kavanaugh, J.L., and Cuffey, K.M. 2003. Space and time variation of $\delta^{18}O$ and δD in Antarctic precipitation revisited. Glob. Biogeochem. Cycles, **17**: 1017. doi: 10.1019/2002GB001910.

Kinnard, C., Zdanowicz, C.M., Fisher, D.A., Isaksson, E., de Vernal, A., and Thompson, L.G. 2011. Reconstructed changes in Arctic sea ice over the past 1,450 years. Nature, **479**: 509–512. doi: 10.1038/nature10581.

Koerner, R.M. 1979. Accumulation, ablation, and oxygen isotope variations on the Queen Elizabeth Islands ice caps, Canada. J. Glaciol. **22**(86): 25–41. doi: 10.3189/S0022143000014039.

Koerner, R., and Russell, R.D. 1979. $\Delta^{18}O$ variations in snow on the Devon Island ice cap, Northwest Territories, Canada. Can. J. Earth Sci. **16**(7): 1419–1427. doi: 10.1139/e79-126.

Kwok, R. 2018. Arctic sea ice thickness, volume, and multiyear ice coverage: losses and coupled variability (1958–2018). Environ. Res. Lett., **13**: 105005. doi: 10.1088/1748-9326/aae3ec.

Lacelle, D. 2011. On the $\delta^{18}O$, δD and D-excess relations in meteoric precipitation and during equilibrium freezing: theoretical approach and field examples. Permafr. Periglac. Process. **22**: 13–25. doi: 10.1002/ppp.712.

Lecavalier, B.S., Milne, G.A., Vinther, B.M., Fisher, D.A., Dyke, A.S., and Simpson, M.J.R. 2013. Revised estimates of Greenland ice sheet thinning histories based on ice-core records. Quat. Sci. Rev. **63**: 73–82. doi: 10.1016/j.quascirev.2012.11.030.

Lecavalier, B.S., Fisher, D.A., Milne, G.A., Vinther, B.M., Tarasov, L., Huybrechts, P., et al. 2017. High Arctic Holocene temperature record from the Agassiz ice cap and Greenland ice sheet evolution. Proceedings of the National Academy of Sciences of the United States of America, **114**: 5952–5957. doi: 10.1073/pnas.1616287114.

Lesins, G., Duck, T.J., and Drummond, J.R. 2010. Climate trends at Eureka in the Canadian High Arctic. Atmosphere-Ocean, **48**(2): 59–80. doi: 10.3137/AO1103.2010.

Lewkowicz, A., and Bonnaventure, P. 2011. Equivalent elevation: a new method to incorporate variable surface lapse rates into mountain permafrost modelling. Permafr. Periglac. Process. **22**(2): 153–162. doi: 10.1002/ppp.720.

Lorius, C., and Merlivat, L. 1977. Distribution of mean surface stable isotope values in East Antarctica: observed changes with depth in the coastal area. Int. Assoc. Hydrol. Sci. Publ., **118**: 127–137 (Symposium at Grenoble 1975 — Isotopes and Impurities in Snow and Ice).

Marsh, J.H. 2015. Queen Elizabeth Islands. The Canadian Encyclopedia. Historical Foundation of Canada. Toronto, Ontario, Canada.

Maxwell, J.B. 1981. Climatic regions of the Canadian Arctic islands. Arctic, **34**(3): 225–240.

Mekis, E., and Hogg, W.D. 1999. Rehabilitation and analysis of Canadian daily precipitation time series. Atmosphere-Ocean, **37**(1): 53–85. doi: 10.1080/07055900.1999.9649621.

Merlivat, L., and Coantic, M. 1975. Study of mass transfer at the air-water interface by an isotopic method. J. Geophys. Res. **80**: 3455–3464. doi: 10.1029/JC080i024p03455.

Merlivat, L., and Jouzel, J. 1979. Global climatic interpretation of the deuterium-oxygen 18 relationship for precipitation. J. Geophys. Res. **84**: 5029–5033. doi: 10.1029/JC084iC08p05029.

Mernild, S.H., and Liston, G.E. 2010. The influence of air temperature inversions on snowmelt and glacier mass balance simulations, Ammassalik Island, southeast Greenland. J. Appl. Meteorol. Climatol. **49**(1): 47–67. doi: 10.1175/2009JAMC2065.1.

Millan, R., Mouginot, J., and Rignot, E. 2017. Mass budget of the glaciers and ice caps of the Queen Elizabeth Islands, Canada, from 1991 to 2015. Environ. Res. Lett. **12**: 024016. doi: 10.1088/1748-9326/aa5b04.

Peixóto, J.P., and Oort, A.H. 1983. The atmospheric branch of the hydrological cycle and climate. *In* Variations in the global water budget. *Edited by* A. Street-Perrott, M. Beran, and R. Ratcliffe. D. Reidel Publishing Co., Dordrecht, the Netherlands. pp. 5–66.

Rowley, D.B. 2007. Stable isotope-based paleoaltimetry: theory and validation. Rev. Mineral. Geochem., **66**: 23–52. doi: 10.2138/rmg.2007.66.2.

Serreze, M.C., Barrett, A.P., Stroeve, J.C., Kindig, D.N., and Holland, M.M. 2009. The emergence of surface-based Arctic amplification. The Cryosphere, **3**: 11–19. doi: 10.5194/tc-3-11-2009.

Serreze, M.C., Schnell, R.C., and Kahl, J.D. 1992. Low-level temperature inversions of the Eurasian Arctic and comparisons with Soviet drifting station data. J. Clim., **5**(6): 615–629. doi: 10.1175/1520-442(1992)005<0615:LLTIOT>2.0.CO;2.

Serreze, M.C., and Stroeve, J. 2015. Arctic sea ice trends, variability and implications for seasonal ice forecasting. Philos. Trans. R. Soc. A, **373**: 20140159. doi: 10.1098/rsta.2014.0159. PMID: 26032315.

Sharp, M., Burgess, D.O., Cogley, J.G., Ecclestone, M., Labine, C., and Wolken, G.J. 2011. Extreme melt on Canada's Arctic ice caps in the 21st century. Geophys. Res. Lett. **38**(11): L11501. doi: 10.1029/2011GL047381.

Sharp, M., Burgess, D.O., Cawkwell, F., Copland, L., Davis, J.A., Dowdeswell, E.K., et al. 2014. Remote sensing of recent glacier changes in the Canadian Arctic. *In* Global Land Ice Measurements from Space, Chapter 9. *Edited by* J.S. Kargel, G.J. Leonard, M.P. Bishop, A. Kääb, and B.H. Raup. Praxis-Springer, Chichester, UK. pp. 205–228. doi: 10.1007/978-3-540-79818-7_9.

Sharp, M., Wolken, G., Burgess, D., Cogley, J.G., Copland, L., Thomson, L., et al. 2015. Glaciers and ice caps outside Greenland. *In* State of the climate in 2014. *Edited by* J. Blunden and D.S. Arndt. Bulletin of the American Meteorological Society, Boston, Massachusetts, USA. Vol. 96(7), pp. 135–137. doi: 10.1175/2015BAMSStateoftheClimate.1.

Thomson, L., Zemp, M., Copland, L., Cogley, G., and Ecclestone, M. 2017. Comparison of geodetic and glaciological mass budgets for White Glacier, Axel Heiberg Island, Canada. J. Glaciol. **63**(237): 55–66. doi: 10.1017/jog.2016.112.

Wang, Y., Hou, S., Masson-Delmotte, V., and Jouzel, J. 2009. A new spatial distribution map of $\delta^{18}O$ in Antarctic surface snow. Geophys. Res. Lett. **36**: L06501. doi: 10.1029/2008GL036939.

White, A., and Copland, L. 2018. Area changes of glaciers across Northern Ellesmere Island, Nunavut, between ~1999 and ~2015. J. Glaciol. **64**(246): 609–623. doi: 10.1017/jog.2018.49.

Wohlleben, T.M. 2009. Ice-atmosphere interactions in the Canadian High Arctic: Implications for the thermomechanical evolution of terrestrial ice masses. Ph.D. thesis, Department of Earth and Atmospheric Sciences, University of Alberta, Canada, 225 pp.